Influence of Winding Scheme on the Iron-Loss Distribution in Permanent Magnet Synchronous Machines

Georg von Pfingsten, Simon Steentjes, Marco Hombitzer, David Franck, and Kay Hameyer

Institute of Electrical Machines, RWTH Aachen University, Aachen D-52062, Germany

The influence of the winding scheme [concentrated, single-tooth, distributed (pitched, unpitched)] on the iron-loss distribution in a rotor and stator is to a large extent unknown. At present, windings are primarily selected with respect to back-EMF harmonics and torque fluctuation. In such approaches, the influence of iron losses is disregarded. Moreover, minor loop losses are not covered by most iron-loss models and are therefore ignored. This yields inaccurate results. In particular, for interior permanent magnet machines, the rotor temperature has to be taken into account. For variable-speed drives, losses have to be calculated over the complete operating range. Hence their distribution is studied in this paper for various operating points. The influence of the winding scheme on iron losses and iron-loss distribution is investigated based on finite-element simulations.

Index Terms—**Loss distribution, permanent magnet (PM) synchronous machines, rotor iron losses, stator design, winding scheme.**

I. Introduction

BECAUSE of the strong limitation of battery capacity to date, optimization of the efficiency of electrical machines for various operating points and operation modes ranks first in automotive applications.

The main design limitation of highly advanced traction drives with high power densities and efficiencies is their cooling system [2], i.e., the possibility of heat dissipation. To reach closer to the edge of machine design, extensive knowledge about losses is indispensable. Because of high speeds and concomitantly high electric frequencies in the stated machines, the iron losses are one major loss component. Hence, estimation of iron losses occurring in the machines' stator and rotor parts is indispensable to effectively carry out electromagnetic and thermal design of these electrical machines. The major portion of iron losses is dissipated in the stator, and a smaller part appears in the rotor. However, because of the better cooling capacities of stators and stronger limitation to rotor temperatures due to the constraints of bearings and permanent magnets (PMs) [2], the loss distribution inside the machine is of importance. One way to influence the loss distribution is through adapting the stator design, i.e., trying to influence the loss distribution by the winding scheme. At present, windings are primarily selected with respect to back-EMF harmonics and torque fluctuation. In such approaches, the influence of iron losses is disregarded during the initial design process, and attempts are made to reduce the impact only afterward, e.g., by segmenting the magnets in a permanent magnet PM machine [3], [4] to limit eddy current losses inside the magnets. In this paper, the effect of the winding scheme [single-tooth, distributed (pitched, unpitched)] on iron-loss distribution in rotor and stator is analyzed. In [5], the iron-loss distribution for two operating points is presented. Since for variable-speed drives the losses strongly depend on the operation mode, the distribution of iron losses is investigated for various operating points. The machine used for this paper is a V-shaped PM synchronous machine (VPMSM) with internal magnets designed as propulsion drive of an electric sports car (Fig. 1). In [6], it is suggested that the number of slots (due to slot harmonics) has a significant impact on rotor iron losses of a surface-mounted machine. However, for the machines studied in [6], the PM losses contribute the highest to the rotor losses. For the studied VPMSM, the PM losses are negligible. Therefore, here the iron losses are studied.

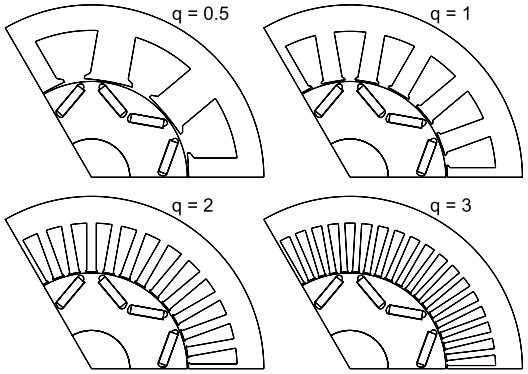

Fig. 1. Cross sections of the studied machines.

II. Design of Studied Machines

A. Rotor

The rotor of the machine is designed to allow a maximum speed of 18 000 min^{-1}. From structural finite-element analysis, a VPMSM rotor with three pole pairs was found to be the best suited. This design leads to electric base frequencies f of up to 900 Hz. For all investigated stators and windings, the rotor design was identical (Fig. 1).

B. Stator

The different stators of the machines were designed to ensure equal magnetic resistances for stators with different q values (q: number of slots N per pole and phase). Therefore, the product of q and width of one stator tooth w_t is kept

Manuscript received August 2, 2013; revised September 21, 2013 and October 11, 2013; accepted October 21, 2013. Date of current version April 4, 2014. Corresponding author: G. von Pfingsten (e-mail: georg.vonpfingsten@iem.rwth-aachen.de).

Color versions of one or more of the figures in this paper are available online at http://ieeexplore.ieee.org.

Digital Object Identifier 10.1109/TMAG.2013.2288433

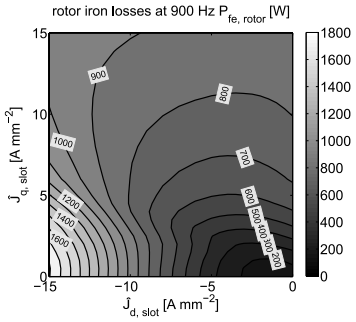

Fig. 2. Simulated rotor iron losses for a stator with $q = 2$, $w = \tau_p$ at one frequency and different current densities.

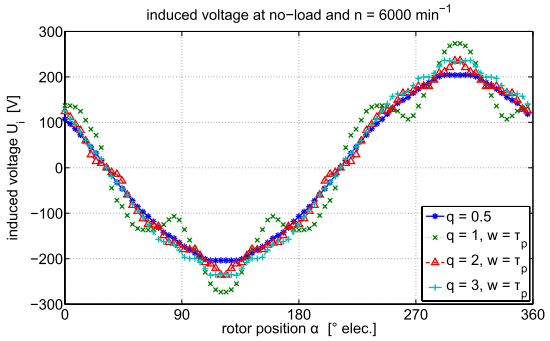

Fig. 3. Induced voltages at no load for all stators with no winding pitch.

constant. However, the area sum of the winding windows of the different stators differs slightly with a maximum of 8% due to increased stator tip height at larger stator teeth (small q).

The minimal air gap was fixed to 0.7 mm. Considering the stator with $q = 0.5$, high distortions in the induced voltage waveform and excessively increased short-circuit magnetic flux paths inside each tooth are apparent. Therefore the stators' pole shape was changed, resulting the air gap to reach the minimal distance of 0.7 mm only in the tooth's center. At the tooth's edges larger distances occur. This leads to lower magnetic flux and with $q \cdot w_t = \text{const}$ to lower magnetic flux densities, and hence to lower maximum torques and iron losses. The number of slots N was varied from 9 to 54, which equals a variation of q from 0.5 to 3. Except for $q = 0.5$, which corresponds to a concentrated single-tooth winding, distributed windings with integer q ($q = 1,\ 2,$ and 3) are evaluated. For the distributed windings, different coil pitches w were simulated. The outer dimensions of the stator stack and the overall stator magnetic resistances were kept constant. For all stators, the design voltage was fixed to 370 V. The number of turns was adjusted to yield this voltage at 6000 min^{-1} and 100 Nm without going into field-weakening. Up to three coil pitches w/τ_p (with τ_p being the pole pitch) were studied for each q. Overall, nine different stator designs were analyzed, see Table I.

C. Winding Design

Fig. 2 shows the simulated iron losses for one machine at one frequency for different current densities. It is apparent that the rotor iron losses are highly dependent on the d-axis current. The need for field-weakening, and therefore d-currents, is

TABLE I
ROTOR VERSUS OVERALL IRON LOSSES

Stator	$P_{fe,rotor}/P_{fe}$		
	min.	max.	max. at
$q = 0.5$	9 %	30 %	8,000 to 18,000 min^{-1}
$q = 1, w = \tau_p$	5 %	24 %	14,000 to 18,000 min^{-1}
$q = 1, w = \frac{2}{3} \cdot \tau_p$	5 %	24 %	13,000 to 18,000 min^{-1}
$q = 2, w = \tau_p$	2 %	12 %	8,000 to 10,000 min^{-1}
$q = 2, w = \frac{5}{6} \cdot \tau_p$	2 %	11 %	7,000 to 10,000 min^{-1}
$q = 2, w = \frac{4}{6} \cdot \tau_p$	2 %	12 %	8,000 to 11,000 min^{-1}
$q = 3, w = \tau_p$	1 %	7 %	6,000 to 11,000 min^{-1}
$q = 3, w = \frac{8}{9} \cdot \tau_p$	1 %	7 %	6,000 to 10,000 min^{-1}
$q = 3, w = \frac{7}{9} \cdot \tau_p$	1 %	7 %	6,000 to 10,000 min^{-1}

dependent on the voltage level and the winding design. Noting this, the machines' operating points are obtained from the FEM results by transforming from the current plane to torque T and speed n maps. Field weakening is accounted for with a maximum stator line-to-line voltage of 370 V. When leaving the base-speed (maximum torque per ampere: MTPA [7]) region, the smallest current that does not lead to exceeding the voltage limit while yielding the desired torque is calculated. To achieve comparable results, the number of turns was adjusted in such a way that, at 100 Nm and 6000 min^{-1}, the design voltage is reached with the MTPA current. However, the desired 100 Nm could hardly be reached with the $q = 0.5$ stator. This is due to the increased air-gap size on the tooth edges (Fig. 1). Fig. 4(a) depicts the occurring rotor iron losses using a stator with $q = 2$, $w = \tau_p$. It is apparent that the highest rotor iron losses are dissipated at the highest possible torque at maximum speed.

III. FEM SIMULATIONS

For the different stator–rotor combinations, detailed 2-D FEM simulations with 90 angular steps per electric period were conducted using the in-house FE software package pyMoose [8]. For each combination, the d- and q-axis current densities in the slots, $\hat{J}_{d,\text{slot}}$, $\hat{J}_{q,\text{slot}}$, were varied in 21 steps, resulting in a current plane (Fig. 2). The relative motion between the rotor and stator imposes the use of a time-stepping procedure. Single-valued magnetization curves have been used; thereby saturation effects originating from the nonlinear material behavior are included. Second-order effects, originating from hysteresis behavior, are neglected. Iron losses in the laminated stator and rotor cores are estimated *a posteriori* using the local waveforms of the magnetic flux densities in each element using the extended IEM formula (1) detailed in [1] and [9]–[11]

$$P(\hat{B}, f) = a_1 \left(1 + \frac{B_{\min}}{B_{\max}} \cdot (r_{\text{hyst}} - 1)\right) \cdot \sum_{n=1}^{\infty} \left(\hat{B}_n^{\alpha} f_n\right) + a_2 \sum_{n=1}^{\infty} \left(\hat{B}_n^2 f_n^2\right) + a_2 a_3 \hat{B}^{(a_4+2)} f^2 + a_5 \left(1 + \frac{B_{\min}}{B_{\max}} \cdot (r_{\text{excess}} - 1)\right) \cdot \sum_{n=1}^{\infty} \left(\hat{B}_n f_n\right)^{1.5}. \quad (1)$$

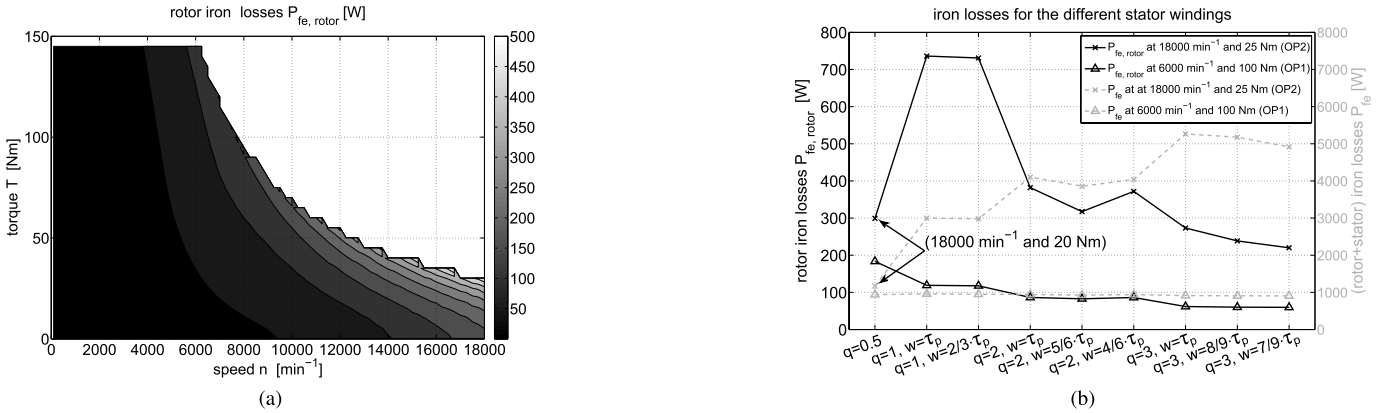

Fig. 4. (a) Simulated rotor iron losses for a stator with $q = 2$, $w = \tau_p$, transformed onto a torque versus speed map. (b) Comparison of rotor iron losses for different stators in two operating points.

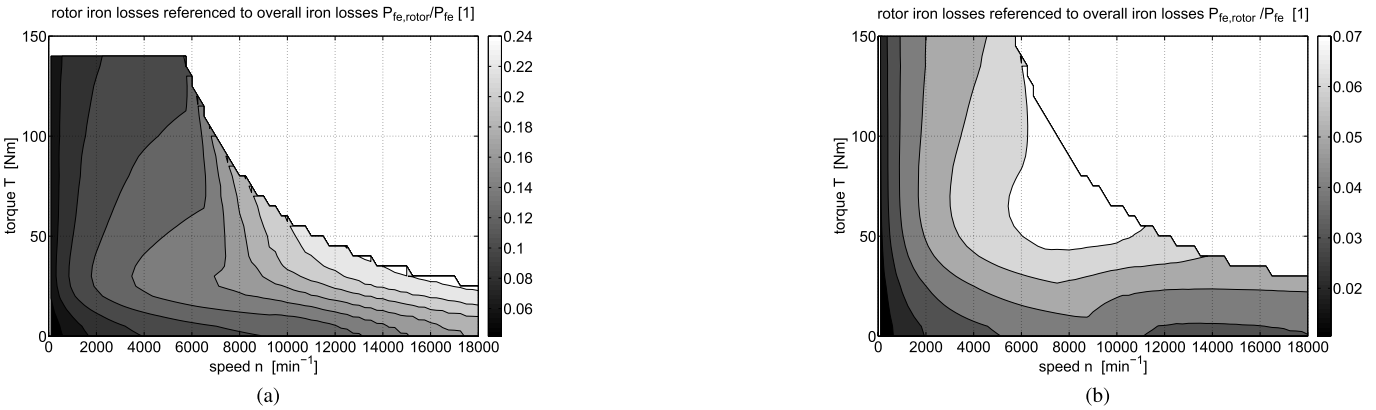

Fig. 5. Rotor iron losses divided by overall iron losses for (a) $q = 1$, $w = \tau_p$ and (b) $q = 3$, $w = \tau_p$.

Thereby, the eddy current loss description is phenomenologically extended to account for the increased losses at high frequencies and flux densities. An exact loss calculation would require the solution of the diffusion equation combined with a dynamic hysteresis model [12]. However, because of infeasible computation times using this approach, iron losses were calculated during postprocessing. The iron losses were subsequently subdivided into rotor and stator iron losses. For the geometry of the stator with $q = 2$ and $w = \tau_p$, the rotor iron losses are shown in Fig. 2 at one frequency and different current densities.

IV. Analysis of the Iron-Loss Distribution

The rotor iron losses are evaluated at 6000 min^{-1} and 100 Nm (transition point between MTPA and field-weakening: OP1) as well as at 18 000 min^{-1} and 25 Nm (high torque at maximum speed: OP2).

In Fig. 4(b), the rotor iron losses are shown for each stator design at OP1 and OP2. At 18 000 min^{-1}, the machine with $q = 0.5$ could only reach 20 Nm. When leaving this point, it becomes clear that the rotor iron losses tend to reach lower values with a higher number of slots. For $q = 1$ (18 slots), 736 W is simulated, whereas for $q = 3$ (54 slots) 273 W is reached. This is equal to a reduction of more than 60%. The influence of winding pitch on the rotor iron losses is rather low. At $q = 1$, a small reduction of less than 1% occurs, whereas at $q = 2$ no steady impact of winding pitch and rotor iron losses could be found. For $q = 3$, a maximum reduction in rotor iron losses of 19.5% could be seen.

In Fig. 3, the induced voltage for the nonpitched machines at no load and 6000 min^{-1} is shown. It could be directly seen that the induced voltage for the machine with $q = 0.5$ is most sinusoidal, which is due to the stator pole form being designed to achieve this (Section II-B). For the other stators without the winding pitch, more sinusoidal voltages are obtained with higher values of q. This shows the good correlation to the analyzed reduction of rotor iron losses at OP1 and OP2. However, the machine with $q = 0.5$ underlines that there is no simple correlation between the induced voltage and rotor iron losses. This is because $q \cdot w_t = \text{const}$ for all machines, resulting in lower magnetic flux densities in the stator material leading to lower stator iron losses.

For stators with $q = 2$ and $q = 3$, a set of multiple stator teeth (lying next to each other) represents a coil group. Once the rotor field enters such a set of teeth, first only one tooth is penetrated by the rotor flux. Thereby, a major amount of the rotor flux runs through this tooth resulting in high magnetic flux densities. When the rotor flux enters the other teeth of such a set, the magnetic flux in the first tooth comes down. The same effect (in different amplitudes) appears at the other teeth of such a set. In stators with q larger than 1, this leads to increasing stator iron losses, resulting

Fig. 6. Iron-loss distribution inside the rotor at 18 000 min^{-1} and 25 Nm for (a) $q = 1$, $w = \tau_p$ and (b) $q = 2$, $w = \tau_p$.

in increased overall iron losses P_{fe} [Fig. 4(b)]. The contrary behavior of stator iron losses to induced voltage underlines the need to consider the iron losses during the whole design process. As a result, the quotient between the rotor and overall iron losses behaves differently for all values of q (Fig. 5). It is apparent that the maximum of the quotient changes from 24% to 7%. Additionally, the position of the maximum shifts from the maximum torque at speeds above 14 000 min^{-1} ($q = 1$, $w = \tau_p$) to maximum torque at about 8000 min^{-1}. The coil pitch has only a minor influence on the iron-loss distribution. In Table I, the maximum quotients and their locations are therefore given for the unpitched machines.

The local iron-loss distribution in the rotor is, like the overall distribution, highly dependent on the stator design. In Fig. 6, the rotor iron losses are shown at OP2 for stators with $q = 1$, $w = \tau_p$ and $q = 2$, $w = \tau_p$. It is apparent that the regions in which high iron losses (over 200 W $\cdot$ kg^{-1}) deplete are larger in area (volume) and amplitude for $q = 1$, $w = \tau_p$ (Fig. 3) compared to $q = 2$, $w = \tau_p$ (Fig. 3). Once higher stator slot numbers are considered, rotor iron losses tend to originate closer to the rotor surface.

V. Conclusion

This paper presented a detailed study of the loss distribution inside a machine. An extended iron-loss formula was used, which was proven to be able to handle rotor-specific loss effects. Using this iron-loss model, the local loss distribution inside the rotor was analyzed. Most iron losses originated close to the air gap. It was shown that the iron losses generated inside the rotor and stator were highly dependent on the number of stator slots. However, the stator geometry with concentrated windings ($q = 0.5$) was not completely suited for the given requirements (resulting in lower flux and flux densities). Therefore, the significance of the following findings should be discussed in future for this winding setup. The initial results for PM machines with concentrated windings were presented in [13]. With a higher number of (smaller) stator slots, less rotor iron losses and higher stator iron losses are dissipated. Accordingly, the relation between rotor and stator iron losses and the iron-loss distribution are highly dependent on the number of stator teeth for machines with integer q. The winding pitch was found to have only a minor effect on the iron losses and their distribution.

Overall, the winding scheme offers the possibility to influence the iron-loss distribution inside the machine. Detailed knowledge of the interdependence of the winding scheme, harmonics, and iron losses enables a differentiated design approach to improve electrical machine efficiencies and the operating limits. The next steps of this research work will focus on experimental validation of the obtained results.

Acknowledgment

This work was supported by the cooperative project e-generation which is funded by the German Federal Ministry of Education and Research under Grant 13N11867.

References

[1] S. Steentjes, G. von Pfingsten, M. Hombitzer, and K. Hameyer, "Iron-loss model with consideration of minor loops applied to FE-simulations of electrical machines," *IEEE Trans. Magn.*, vol. 49, no. 7, pp. 3945–3948, Jul. 2013.

[2] J. Pyrhonen, T. Jokinen, and V. Hrabovcova, *Design of Rotating Electrical Machines*. New York, NY, USA: Wiley, 2008.

[3] K. Yamazaki and Y. Fukushima, "Effect of eddy-current loss reduction by magnet segmentation in synchronous motors with concentrated windings," *IEEE Trans. Ind. Appl.*, vol. 47, no. 2, pp. 779–788, Apr. 2011.

[4] P. Sergeant and A. V. den Bossche, "Segmentation of magnets to reduce loss in permanent-magnet synchronous machines," *IEEE Trans. Magn.*, vol. 44, no. 11, pp. 4409–4412, Nov. 2008.

[5] K. Yamazaki, "Torque and efficiency calculation of an interior permanent magnet motor considering harmonic iron losses of both the stator and rotor," *IEEE Trans. Magn.*, vol. 39, no. 3, pp. 1460–1463, May 2003.

[6] E. Fornasiero, N. Bianchi, and S. Bolognani, "Slot harmonic impact on rotor losses in fractional-slot permanent-magnet machines," *IEEE Trans. Magn.*, vol. 59, no. 6, pp. 2557–2564, Jun. 2012.

[7] R. De Doncker, D. W. J. Pulle, and A. Veltman, *Advanced Electrical Drives: Analysis, Modeling, Control*, New York, NY, USA: Springer-Verlag, 2011.

[8] RWTH Aachen University, Aachen, Germany. (2013, Aug. 8). *Homepage of the Institute of Electrical Machines* [Online]. Available: http://www.iem.rwth-aachen.de

[9] S. Steentjes, M. Leßmann, and K. Hameyer, "Semi-physical parameter identification for an iron-loss formula allowing loss-separation," *J. Appl. Phy.*, vol. 113, no. 17, pp. 17A319-1–17A319-5, 2013.

[10] F. Fiorillo and A. Novikov, "Power losses under sinusoidal, trapezoidal and distorted induction waveform," *IEEE Trans. Magn.*, vol. 26, no. 5, pp. 2559–2561, Sep. 1990.

[11] G. Bertotti, A. Canove, M. Chiampi, D. Chiarabaglio, F. Fiorillo, and A. M. Rietto, "Core los prediction combining physical model with numerical field analysis," *J. Magn. Mat.*, vol. 133, pp. 647–650, Jan. 1994.

[12] S. E. Zirka, Y. I. Moroz, P. Marketos, and A. J. Moses, "Viscosity-based magnetodynamic model of soft magnetic materials," *IEEE Trans. Magn.*, vol. 42, no. 9, pp. 2121–2132, Sep. 2006.

[13] H. VuXuan, D. Lahaye, H. Polinder, and J. A. Ferreira, "Improved model for design of permanent magnet machines with concentrated windings," in *Proc. Electr. Mach. Drives Conf.*, 2011, pp. 948–954.